THERMAL ENVIRONMENT IMPROVEMENT OF UNDERGROUND MINE TUNNELING FACE USING ENHANCED GEOTHERMAL SYSTEM TECHNOLOGY

by

Zeyu SUN[a], Xingxin NIE[a*], Jinjiang LIU[a], Xin ZHANG[a,b*], Shudu ZHANG[a], Min YANG[a], Zhao WANG[a*], Yibo LOU[c], Ting GUO[c], Xiaoxin LUO[c], and Tong GUO[d]

[a] School of Resources Engineering,
Xi'an University of Architecture and Technology, Xi'an, Shaanxi, China
[b] School of Environmental and Municipal Engineering,
Xi'an University of Architecture and Technology, Xi'an, Shaanxi, China
[c] Shaanxi Metallurgical Design and Research Institute Co., Ltd., Xi'an, Shaanxi, China
[d] Zhashui Qintong Construction Co., Ltd., Shangluo, Shaanxi, China

Original scientific paper
https://doi.org/10.2298/TSCI230305132S

To solve the problem of high temperature thermal damages to the mine underground driving working face of a dry-hot-rock-enriched area, an active cooling method for fracturing water injection of the surrounding rock of the deep mine is proposed based on analysis of the heat dissipation mechanism of the surrounding rock. An artificial thermal reservoir is formed in the high temperature rock mass around the tunneling roadway by stimulation, such as a high pressure crack, and the heat energy of the surrounding rock is extracted by heat exchange of the heat-carrying fluid and the high temperature rocks mass to reduce the ambient temperature of the roadway. The design of a downhole water injection cooling system based on enhanced geothermal system technology is presented and a simplified enhanced geothermal system heats collection model is used for fluid-enclosure. Numerical simulation of the temperature field of the rock coupling shows that the temperature of the surrounding rock can be effectively reduced by increasing the water injection speed and fracture porosity, and improvement of the underground thermal environment can improve the working efficiency. For a water injection rate of 14 m/s and porosity of 0.18, the average cross-section temperature was 41.95 ℃, which is nearly 5 ℃ lower than the original rock temperature of 46.85 ℃.

Key words: *mine thermal environment, active cooling, hydraulic fracturing, hot rock*

Introduction

Metal mine resources play a significant role in global economic development [1]. The western region of China are rich in mineral resources and has great mining potential. However, there are many hot rocks in the deep part of the mine due to the particularity of the location, the intensive heat transfer of the hot rock surface and air-flow, with the heat and exhaust gas produced by diesel equipment during excavation, as a result that can create an intolerable hot and humid environment that negatively impacts the performance [2]. It has greatly reduced the production efficiency as well as the personal safety of the underground workforce [3-5]. The

* Corresponding authors, e-mail: niexingxin@xauat.edu.cn, 2601084634@qq.com, wangzhao@xauat.edu.cn

technical specifications for ventilation systems used in underground mines stipulate the air temperature in underground working places shall not exceed 28 °C [6, 7]. Therefore, effective technical measures are required to control the high temperature problem of the driving face caused by heat dissipation from hot rocks in the deep part of the mine.

Mine cooling strategies includes both artificial and non-artificial refrigeration technology [8, 9]. Non-artificial cooling is mainly achieved by increasing ventilation in strong shafts and alleys, careful planning of the ventilation networks, avoiding heat sources, and isolating high temperature surrounding rock [8]. Artificial strategies used in some mines mainly include cooling systems with refrigerated water or ice-making [9-11]. Although these measures can also control downhole cooling, these systems have high operation and maintenance costs as well as a high failure rate, limiting the application of these systems. In addition, these studies also commonly neglect life-of-mine water planning, and mining development and production plans [12]. These cooling measures are based on passive cooling, and the active control of the main heat source could potentially reduce costs [13].

To solve the problems of high energy consumption and high humidity in deep well cooling, some scholars also carried out relevant research [14-19]. Such as a deep well adsorption cooling system based on a heat storage filling body [14], converts mine heat damage into heat energy [15], improves energy recycling efficiency [16], and optimizes the ventilation system by using CFD [17]. Also the thermodynamic performance of compression refrigerator for deep mine [18], and new method to control high temperature in mines [19]. In addition heat dissipation from surrounding rock, heat is also released from mechanical and electrical equipment as well as from ore in transport, which makes the thermal environment inside the mine more complex, and there are also more thermal hazards. The passive cooling technology is typically used to reduce this heat [20-22]. However, active cooling technology is required to control the heat dissipation of the surrounding rock in order to more efficiently providing mine cooling. Effective control of this heat can greatly reduce the downhole temperature. Most geothermal energy in China is found in dry and hot rocks at depths of 3000-10000 meters (hot rocks without water or steam, with temperatures ranging from 15-6 °C) [23, 24]. Therefore, how to reduce the temperature of deep wells is currently one of the primary problems to be solved.

In this paper, an enhanced geothermal system (EGS) was used for deeply research [25]. The use of geothermal mining technology to exploit heat energy in underground surrounding rocks can greatly reduce the cost of cooling. It provides a feasible strategy to improve the underground working environment of a mine with high rock temperature.

Methods

Working principle of EGS technology

In an EGS, heat is extracted from low permeability and low porosity strata (dry hot rock) by creating a subsurface fracture system to which water can be added through injection wells [26]. Unlike traditional hydrothermal geothermal resources, thermal rock resources are rocks with low permeability [27], and typically require artificial fracture to form connected thermal reservoirs. The engineering processes includes drilling into the rock mass and using hydraulic fracturing technology to create a thermal reservoir with connected cracks. The injection well and the production well are connected through the thermal reservoir, the full heat exchange of the fluid with the high temperature rocks mass in the thermal reservoir. The heat energy is extracted to the surface through the production well. Thus, the use of an EGS may be an effective method to exploit geothermal resources for heat energy as well as a strategy to increase mining production efficiency by improving the underground thermal environment [25].

Design of active cooling scheme

With heat transfer analysis of surrounding rock, a scheme of hydraulic fracturing and cooling of underground surrounding rock using EGS technology was designed. The active cooling design is used to solve the problem of high temperature in a mine due to surrounding rock heat dissipation. The design includes an underground circulation heat transfer system and a downhole water injection system. The downhole water injection system is the core part of the design, and is mainly composed of the water injection well, the water well, and rock mass fracture. The thermal fluid enters the rock mass through the injection pump and then there is heat exchange with the high temperature rock mass. The heat flow after heat transfer is collected through the well circulation heat transfer system, and its heat energy is provided to the user as electric energy or hot water, and the cold water after heat transfer re-enters the water injection well for circulation cooling. The work flow is shown in fig. 1. In this study, EGS was used to enhance the coupling and heat transfer effect of fluid-surrounding rock by hydraulic fracturing of hot rock.

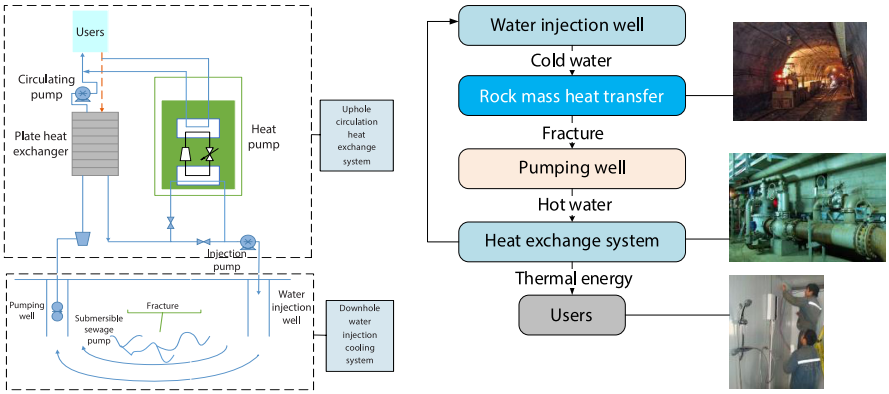

Figure 1. Work flow chart

Analysis of heat dissipation in the surrounding rock of a deep well

There are many influencing factors of downhole heat damage, but heat dissipation from the surrounding rock accounts for the vast majority of the heat in the well. The main factors directly affecting the heat dissipation from the surrounding rock are the density of the surrounding rock, the thermal conductivity of the surrounding rock, the thermal conductivity of the rock, the specific heat capacity of the surrounding rock, and the heat storage coefficient of the surrounding rock. In different mines, the heat dissipation intensity of different scattered heat sources is different, and can change with time [28]. However, the heat dissipation from the surrounding rock of the mine occurs through the whole tunnel of the mine.

Heat exchange between the surrounding rock and air in underground rock is a complex unstable process. A temperature difference between the rock wall and the air-flow in the roadway was given, if the temperature of the original rock is generally high, the heat is transferred from the wall to the air-flow as convective heat release. The heat transfer process inside a rock body is heat conduction. This process can be studied using relevant theories of heat conduction [29]. Fourier's law is calculated [29, 30]:

$$q = \frac{\Phi}{A} = -\lambda \frac{\mathrm{d}t}{\mathrm{d}x} \tag{1}$$

where Φ is the heat flow through the surface, q [Js^{-1}] – the heat flow per unit surface, A [m^2] – the surface area through which heat passes, λ [°Cm^{-1}] – the thermal conductivity inside the rock mass, and dt/dx – the temperature gradient along the x-direction.

A small ladder block was used as the research object in this study. Without considering an internal heat source, the heat corresponding to the temperature change of the small block should be equal to the algebraic sum of the inflow and outflow heat flow in three directions. It can be seen that the polar partial differential equations of unstable heat conduction in 3-D space are calculated [30, 31]:

$$\frac{k}{pc}\left(\frac{\partial^2 t}{\partial r^2}+\frac{1}{r}\frac{\partial t}{\partial r}+\frac{1}{r^2}\frac{\partial^2 t}{\partial \phi^2}+\frac{\partial^2 t}{\partial z^2}\right)=\frac{\partial t}{\partial \tau} \tag{2}$$

where k [Js^{-1}m^{-1}°C^{-1}] is the thermal conductivity of the trapezoidal block, t [°C] – the temperature of the trapezoidal block, m [kg] – the mass of the trapezoidal block, c [Jkg^{-1}°C^{-1}] – the specific heat capacity of the trapezoidal block, and τ [second] – the heat conduction time of the trapezoidal block.

Compared with radial geothermal gradient, the geothermal gradient in the axial and annular directions can be negligible, it is calculated [30, 31]:

$$\frac{\partial t}{\partial z}=\frac{\partial^2 t}{\partial z^2}=0,\ \frac{\partial t}{\partial \phi}=\frac{\partial^2 t}{\partial \phi^2}=0 \tag{3}$$

The 3-D thermal differential is calculated [30, 31]:

$$\frac{k}{pc}\left(\frac{\partial^2 t}{\partial r^2}+\frac{1}{r}\frac{\partial t}{\partial r}\right)=\frac{\partial t}{\partial \tau} \tag{4}$$

where $\alpha = k/pc$ is the temperature coefficient, and the introduction of the temperature coefficient into the aforementioned equation. It is calculated [30, 31]:

$$\alpha\left(\frac{\partial^2 t}{\partial r^2}+\frac{1}{r}\frac{\partial t}{\partial r}\right)=\frac{\partial t}{\partial \tau} \tag{5}$$

Using this equation and the convective heat transfer equation, the unstable heat transfer coefficient reflecting the heat exchange between surrounding rock and air-flow in roadway can be introduced, which can be used as the basis to improve the thermal environment of the heading face.

The calculation of convective heat transfer is calculated [30, 31]:

$$q'=\frac{\Phi'}{A}=h(t_w-t_f) \tag{6}$$

where A [m^2] is the surface area of the rock mass, Φ [W] – the convective heat transfer, q' [Jm^{-2}s^{-1}] – the heat flux density, h [Wm^{-2}°C^{-1}] – the surface heat transfer coefficient, t_w [°C] – the temperature of the surface of the rock mass, and t_f [°C] – the wind flow temperature.

Establishment of physical model and mathematical model

The tunnel in the middle section of the underground –1250 m of the gold mine in Qinghai Province is used as the research object, which is located in an area of hot rock enrichment area in western China. The surrounding rock body is length × width × height = 150 m × × 30 m × 25 m. The middle part is the driving tunnel, the straight wall is 2.5 m, the height of the arch is 2 m. The bottom of the tunnel is 3 m from the bottom of the surrounding rock, the cross-section of the tunnel is a semi-circular arch, and the height of the section is 4.5 m. The initial temperature of the surrounding rock of the area is 46.85 °C (320 K).

The rock mass part is coupled and analyzed to simplify the calculation, and the injection well and the water taking well are omitted. The simplified physical model is shown in fig. 2. The cold water is injected from the left side rock wall of the model through 25 water injection holes. Geometron is used to create the geometric model, then the mesh is divided, and the model is imported into FLUENT software to set and solve the boundary conditions.

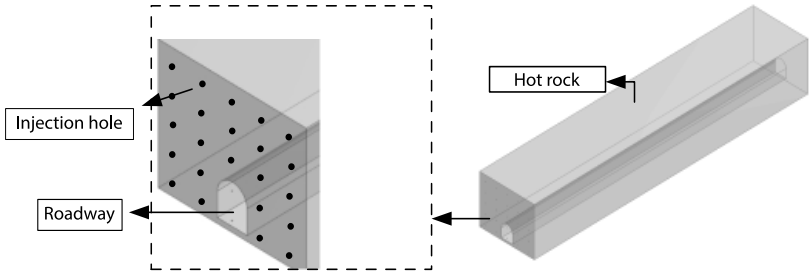

Figure 2. Simplified physical model

The basic assumptions of the model are:

– the fluid is incompressible,
– the water is injected at constant speed and at unchanged direction,
– the influence of the thermal radiation of the surrounding rock on the cooling system is ignored, and
– the thermal resistance at the junction of the fluid and the surrounding rock is ignored.

The basic parameter settings are listed in tab. 1.

Table 1. Model basic parameters

Parameter	Physical meaning	Numerical value
ρ_s	Hot rock density	2750 kg/m^3
C_s	Hot rock specific heat capacity	0.89 kJ/kgK
λ_s	Thermal conductivity of rock	2.2 W/mK
C_f	Specific heat capacity of injected water	4200 J/kgK

The rock mass temperature field is calculated [32]:

$$\rho_y c_{p,y} \frac{\partial T_y}{\partial t} = \lambda_y \nabla^2 T_y + W \tag{7}$$

where ρ_y [kgm^{-3}] is the density of the surrounding rock, T_y [K] – the temperature of the rock mass, $c_{p,y}$ [Jkg^{-1}K^{-1}] – the specific heat capacity of the rock mass, λ_y [Wm^{-1}K^{-1}] – the heat transfer coefficient of the rock mass, and W [Wm^{-3}] – the heat source item.

The temperature of fractured water is calculated [33]:

$$c_{p,s} \frac{\partial(\rho_s T_s)}{\partial t} = \lambda_s \nabla^2 T - c_{p,s}(\rho_s k_f \nabla p_i T_s)_i + \frac{\lambda_y}{\delta}(T_{rb} - T_s) \tag{8}$$

where λ_s [Wm^{-1}K^{-1}] is the heat transfer coefficient of water, $c_{p,s}$ [Jkg^{-1}K^{-1}] – the specific heat capacity of water, ρ_s [kgm^{-3}] – the density of water, λ_y [Wm^{-1}K^{-1}] – the heat transfer coefficient of rock mass, T_s [K] represents the temperature of water, and T_{rb} [K] – the rock temperature value of the crack edge.

Fractured water seepage is calculated [34]:

$$d_f S_f \frac{\partial p}{\partial t} + \nabla \tau \left(-d_f \frac{k_f}{\eta} \nabla p \right) = -d_f \frac{\partial e_f}{\partial t} + Q_f \tag{9}$$

where K_f [m^2] is the fracture permeability coefficient, d_f [Pa^{-1}] – the fracture water storage coefficient, Q_f – the flow exchange between the rock mass and the fracture and e_f – the overall strain of the fracture.

Setting of boundary conditions and selection of calculation methods

The boundary conditions and initial conditions of the model were set:

– The surrounding rock mass conditions are set as porous media area, the wall surface has no slip, and porosity is 0.06, 0.12, or 0.18. The density of the rock mass is 2750 kg/m^3, and the specific heat is 0.89 kJ/kgK.
– The inlet and outlet and wall boundary conditions are when the velocity inlet boundary is adopted, the water flow rate is 0.8 m/s, 1.1 m/s, and 1.4 m/s, and the water injection temperature is 15 °C. The wall of the roadway surrounding rock is considered mainly sandstone, and the temperature is 46.85 °C (320 K).

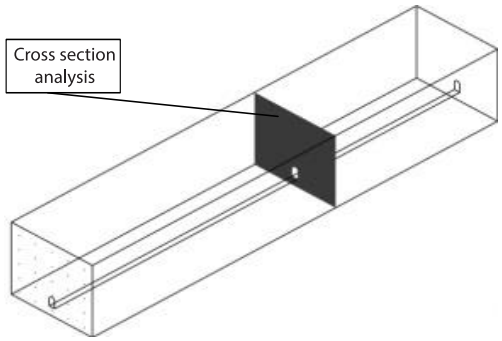

Figure 3. Cross-section model at uniform porosity

– The calculation is performed using three main equations: the continuity equation, the momentum equation, and the energy equation.

A total tetrahedral mesh is adopted with 5731575 grid elements and 1001791 nodes. Temperature is studied by analysis of the longitudinal and cross-section temperature fields under different conditions. A uniform porosity cross-section was selected as shown in fig. 3.

Results and discussion

Effect of water injection speed on cooling effect

The porosity was set to be stable at 0.12, and the water velocity at the inlet was set as 0.8 m/s, 1.1 m/s, or 1.4 m/s, as shown in fig. 4.

As shown in fig. 4, the temperature field of the cross-section of the surrounding rock is distributed symmetrically. For the inlet water velocity of 0.8 m/s, the average temperature of the cross-section is 44.65 °C (317.8 K), with a temperature difference of the section of 6.34 °C. The temperature distribution and cooling effect of the cross-section of the flow field is not good, and the distribution of the high temperature area is obvious. With increased water velocity, the cooling effect of the flow field becomes obvious. After the velocity is increased, the temperature of the upper half of the section is reduced and the temperature is uniform. When the velocity is 1.1 m/s, the average temperature of the section is 43.15 °C (316.3 K), with a temperature difference of the section of 8.89 °C. When the velocity is 1.4 m/s, the average temperature of the section is 42.45 °C (315.6 K), with a temperature difference of the section of 11.40 °C. The temperature was plotted against the direction of the fracture (z-axis) for the aforementioned three velocity conditions, as shown in fig. 5.

The corresponding transverse co-ordinates from the water injection mouth to the outlet are 0 ~ –150. Under different injection velocities, along $x = 0$, $y = 0$, 0 ~ –150, the larg-

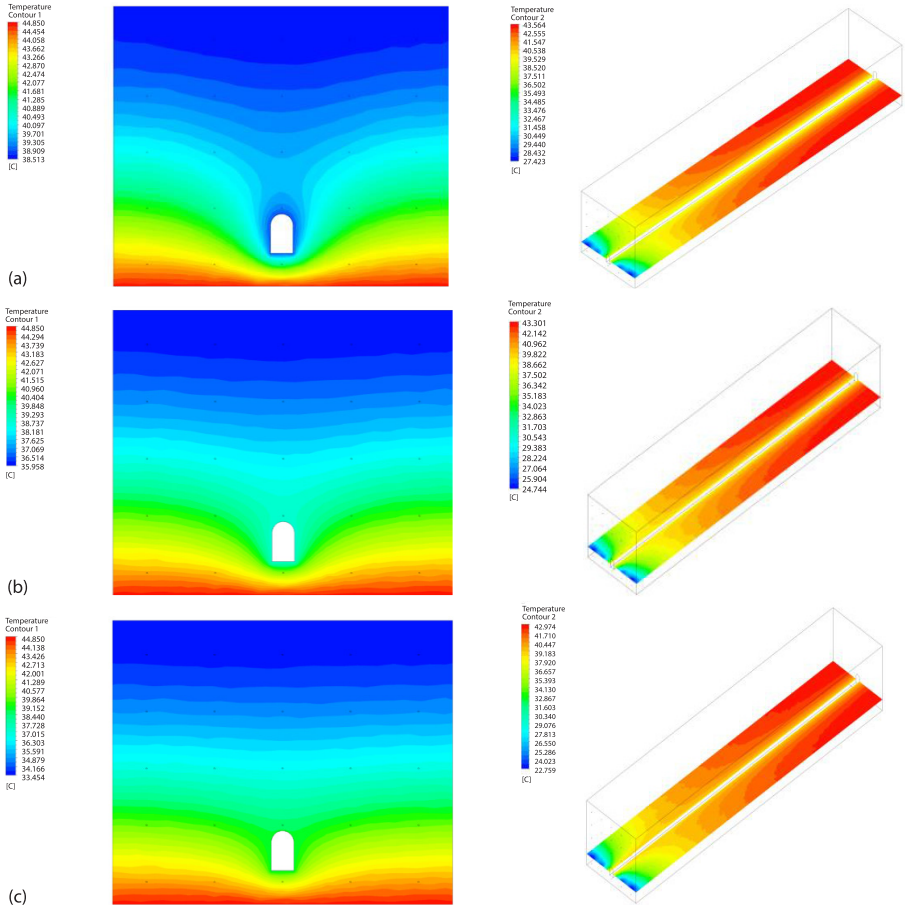

Figure 4. Cloud images of cross-section temperatures at different inlet velocities; (a) cloud image of cross-section temperature distribution at 0.8 m/s, (b) cloud picture of cross-section temperature distribution at 1.1 m/s, and (c) cloud image of cross-section temperature distribution at 1.4 m/s

er the water injection velocity, the lower the corresponding curve at the same position and the better the cooling effect of the surrounding rock. As shown in the figure, at the entrance (z = 0 ~ –20 m), the surrounding rock at the entrance has a lower temperature and exhibits a faster temperature drop. It indicates that good contact and heat transfer between the cold water and hot rock, which makes the cold water to remove the heat from the hot rock more quickly. At z = –60 ~ –20 m, the heat transfer between the water and hot rock is still good, and the temperature drop amplitude of the surrounding rock mass increases. At z = –150 ~ –60 m, with

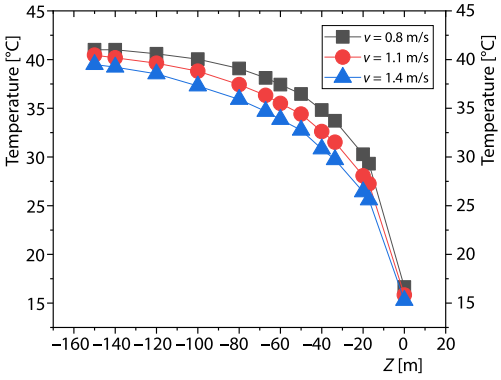

Figure 5. Temperature distribution under different injection velocities

the continuous increase of water injection temperature, the heat exchange amplitude with surrounding rock decreases, and the temperature drop of the surrounding rock decreases. The higher the water injection velocity, the better the cooling effect.

Effect of porosity on cooling effect

The injection velocity of 1.4 m/s was maintained, and the porosity was changed to 0.06 and 0.18, as shown in fig. 6.

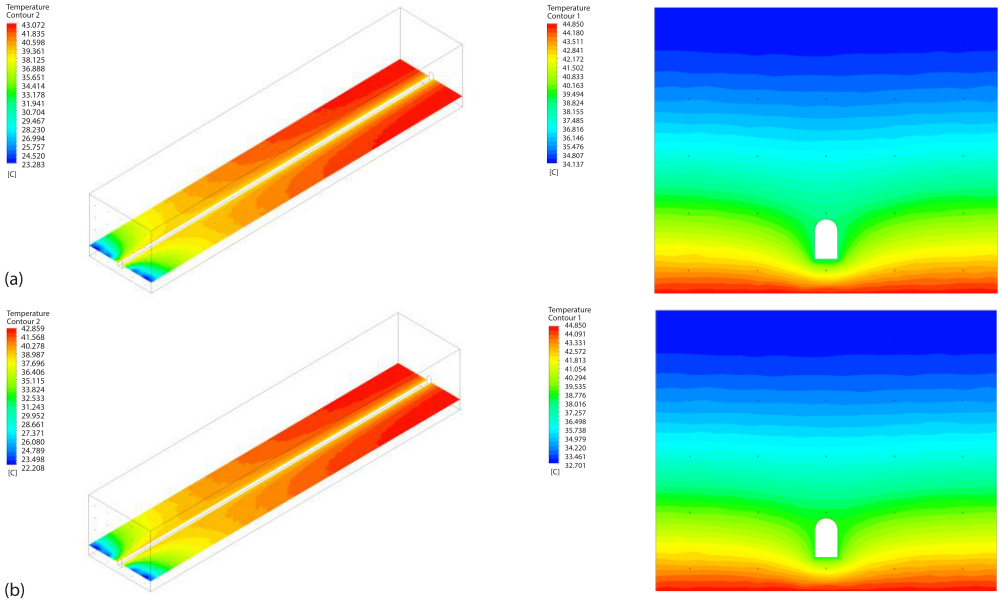

Figure 6. Cross-section temperature at different porosity;
(a) cloud image of cross-section temperature distribution at porosity of 0.06 and
(b) cloud image of cross-section temperature distribution at porosity of 0.18

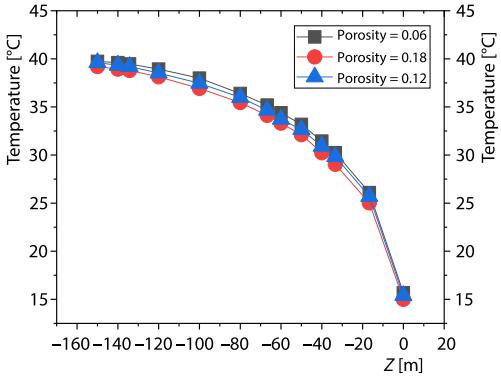

Figure 7. Temperature distribution curve for different porosity

As shown in fig. 7, it has only a slight difference in the temperature distribution curve at different porosity. For porosity of 0.06, the average cross-section temperature is 40.05 °C (316.2 K), with the cross-section temperature difference of 10.71 °C. For porosity of 0.12, the average cross-section temperature is 42.45 °C (315.1 K), with the cross-section temperature difference of 11.40 °C. For porosity of 0.18, the average cross-section temperature is 41.95 °C (315.1 K), with the cross-section temperature difference of 12.15 °C.

For the three cases, the curve is obtained along the line of $x = 0$, $y = 0$, and $z = 0 \sim -150$. The curve is higher than the curve at porosity of 0.12 and 0.18 when the porosity is 0.06, and the cooling effect is weak. At constant porosity, the cooling process along the z-axis roughly exhibits two-stages, $z = 0 \sim -20$ m and $z = -150 \sim -20$ m. In the first stage, the porosity plays a major role due to the increased contact area with the rock mass, which results in a bigger effect

to reduce temperature. In the second stage, with full exchange of heat between the water and the rock mass, the ability of the injected water to remove the heat of the surrounding rock is gradually reduced. The slope of the curve tends to be gentle in the second stage. The larger the porosity, the more obvious the cooling effect.

Conclusions

With geothermal energy utilization and heat transfer of surrounding rock, an active cooling scheme for high temperature mine water injection based on EGS technology is described. The conclusions of this paper can be summarized are as follows.

- A simulation model of a high rock temperature mine using EGS technology was constructed, and the results show that reasonable water injection velocity and suitable fracture porosity can play a good cooling effect.
- At certain porosity, the cooling effect of the surrounding rock increased with increased water injection rate. When the water injection velocity increased from 0.8-1.4 m/s, the cross-sectional temperature was reduced by nearly 2 °C. The water injection velocity can be improved under the maintenance of basic performance and consideration of costs.
- At certain water injection velocity, the cooling effect of the surrounding rock is increased with the increase of the crack porosity. The porosity increased from 0.06-0.18, the temperature difference was almost 1 °C.
- For the water injection and cooling of the mine in a high rock temperature area, the water injection velocity should be increased technically and economically as much as improved the crack porosity of the rock.

Acknowledgment

The work was supported by the Key Research and Development Program of Shaanxi Province of China (No. 2023-YBGY-137) and the College Students' Innovative Entrepreneurial Training Plan Program (No. 202210703024), also supported by the National Natural Science Foundation of China (No. 42272342), and the Natural Science Basic Research Program of Shaanxi (No. 2021JM-350).

References

[1] Wang, S., *et al*., Operation Optimization of a Refrigeration Ventilation System for The Deep Metal Mine, *Case Studies in Thermal Engineering*, *44* (2023), 102817
[2] Xin, S., *et a*l., Application of Data Envelopment Analysis in the Ventilation and Cooling Efficiency Evaluation of Hot Development Headings, *Processes*, *10* (2022), 1375
[3] Nie, X. X., *et a*l., Evaluation of Influencing Level of Deep Wells' Thermal and Humid Environment on Miners' Mental and Physical Safety, *China Safety Science Journal*, *31* (2021), 12, pp. 24-31
[4] Zhang, Z. J., *et al*., Renew Mineral Resource-Based Cities: Assessment of PV Potential in Coal Mining Subsidence Areas, *Applied Energy*, *329* (2023), 20296
[5] Guo, P., *et al*., A Geothermal Recycling System for Cooling and Heating in Deep Mines, *Applied Thermal Engineering*, *116* (2017), Apr., pp. 833-839
[6] Zhang, H. Y., *et al*., Numerical Study on Interactions between Climate Conditions and Diesel Exhaust and Optimization of Auxiliary Ventilation in Underground Mines, *Thermal Science and Engineering Progress*, *37* (2023), 101594
[7] Yang, B., *et al.*, A Review of Ventilation and Environmental Control of Underground Spaces, *Energies*, *15* (2022), 2, 409
[8] Chang, Z. Y., *et al*., Heat Absorption Control Equation and Its Application of Cool-Wall Cooling System in Mines, *Journal of Central South University*, *28* (2021), Oct., pp. 2735-2751
[9] Hu, R., *et al*., Research Status of Supercooled Water Ice Making: A Review, *Journal of Molecular Liquids*, *347* (2022), 118334

[10] Dong, L. J., *et al*., Some Developments Aad New Insights of Environmental Problems and Deep Mining Strategy for Cleaner Production in Mines, *Journal of Cleaner Production*, *210* (2019), Feb., pp. 1562-1578
[11] Cai, M. F., *et al*., Key Engineering Technologies to Achieve Green, Intelligent, and Sustainable Development of Deep Metal Mines in China, *Engineering*, *7* (2021), 11, pp. 1513-1517
[12] Monteiro, C. A., *et al*., A Simulation-Based Water Management Strategy for Life-of-Mine Water Planning, *South African Journal of Industrial Engineering*, *33* (2022), 3, pp. 248-261
[13] Li, Y. F., *et al*., Experimental Study on Heat Transfer Process Optimization of Heat Storage Wall of the Heat Pump in Tunnel Surrounding Rock in the Cold Region, *Geofluids*, *2022* (2022), ID5224154
[14] Chen, L., *et al*., Mechanism of Backfill Thermal Utilization Adsorption Cooling System in Deep Mine, *Journal of China Coal Society*, *43* (2018), 2 pp. 483-489
[15] Menendez, J., *et al*., Feasibility Analysis of Using Mine Water From Abandoned Coal Mines in Spain for Heating and Cooling of Buildings, *Renewable Energy*, *146* (2020), Feb., pp. 1166-1176
[16] Gorman, M. R., Dzombak, D. A., A Review of Sustainable Mining and Resource Management: Transitioning from the Life Cycle of the Mine to the Life Cycle of the Mineral, Resources, *Conservation and Recycling*, *137* (2018), Oct., pp. 281-291
[17] Chen, W., *et al.*, Proposed Split-Type Vapor Compression Refrigerator for Heat Hazard Control in Deep Mines, *Applied Thermal Engineering*, *105* (2016), 25, pp. 425-435
[18] Vives, J., *et al*., Computational Fluid Dynamics (CFD) study to Optimize the Auxiliary Ventilation System in an Underground Mine, *DYNA*, *89* (2022), 221, pp. 84-91
[19] Xu, Y., *et al*., An Investigation into the Effect of Water Injection Parameters on Synergetic Mining of Geothermal Energy in Mines, *Journal of Cleaner Production*, *382* (2023), 135256
[20] Kang, C. H., *et al*., Control Theory and Technology Analysis of High Temperature in Deep Mining, *Safety in Coal Mines*, *47* (2016), 5, pp. 89-93
[21] Wang, H., Zhou, Q. Y., Finite Element Analysis of Surrounding Rock with a Thermal Insulation Layer in a Deep Mine, *Mathematical Problems in Engineering*, *2020* (2020), ID5021853
[22] Zueter, A. F., *et al*., Numerical Study on the Cooling Characteristics of Hybrid Thermosyphons: Case Study of the Giant Mine, Canada, *Cold Regions Science and Technology*, *189* (2021), 103313
[23] Chen, J., Liang, F., Designing multi-Well Lay-Out for Enhanced Geothermal System to Better Exploit Hot Dry Rock Geothermal Energy, *Renewable Energy*, *74* (2015), Feb., pp. 37-48
[24] Wang, Y. Q., *et al*., Geothermal Energy in China: Status, Challenges, and Policy Recommendations, *Utilities Policy*, *64* (2020), 101020
[25] Olasolo, P., *et al*., Enhanced geothermal Systems (EGS): A Review, *Renewable and Sustainable Energy Reviews*, *56* (2016), Apr., pp. 133-144
[26] Liu, Q., *et al*., Multiple-relaxation-Time Lattice Boltzmann Model for Simulating Axisymmetric Thermal Flows in Porous Media, *International Journal of Heat and Mass Transfer*, *137* (2019), July, pp. 1301-1311
[27] Xiao, W., *et al*., Effect of Sodium Oleate on the Adsorption Morphology and Mechanism of Nanobubbles on the Mica Surface, *Langmuir*, *35* (2019), 28 pp. 9239-9245
[28] Lai, J. X., *et al.*, Freeze-Proof Method and Test Verification of a Cold Region Tunnel Employing Electric Heat Tracing, *Tunnelling and Underground Space Technology*, *60* (2016), Nov., pp. 56-65
[29] Nie, X. X., *et al*., Simulation study on the Dynamic Ventilation Control of Single Head Roadway in High-Altitude Mine Based on Thermal Comfort, *Advances in Civil Engineering*, *2019* (2019), ID3975745
[30] Li, C. R., *et al.*, Low and heat Transfer of a Generalized Maxwell Fluid with Modified Fractional Fourier's Law and Darcy's Law, *Computers and Fluid*s, *125* (2016), Nov., pp. 25-38
[31] Zhang, S. B., *et al*., Displacement Characteristics of a Urban Tunnel in Silty Soil by Shallow Tunnelling Method, *Advances in Civil Engineering*, *2020* (2020), ID3975745
[32] Xu, X. H., *et al*., Study on the influence of Fracture Flow on The Temperature Field of Rock Mass with High Temperature, *Case Studies in Thermal Engineering*, *22* (2020), 100755
[33] Abbasi, M., *et al*., Analytical Model for Heat Transfer between Vertical Fractures in Fractured Geothermal Reservoirs during Water Injection, *Renewable Energy*, *130* (2019), Jan., pp. 73-86
[34] Zhao, Y. L., *et al.*, Coupled Seepage-Damage Effect in Fractured Rock Masses: Model Development and a Case Study, *International Journal of Rock Mechanics and Mining Sciences*, *144* (2021), 104822

Paper submitted: March 5, 2023
Paper revised: April 19, 2023
Paper accepted: April 25, 2023